

# Implementation of cooling slots at the pressure side rims of squealer tips

## Original article

### Article history:

Submission date: 24 March 2024

Final revision date: 25 April 2024

Acceptance date: 19 August 2024

Publication date: 31 October 2024

This is the updated version of a paper originally presented at the Global Power and Propulsion Technical Conference, GPPS Chania22, September 20-22, 2022.



### \*Correspondence:

JACV: joaovieira10@hotmail.com

### Peer review:

Single blind

### Copyright:

© 2024 Vieira et al. © This is an open access article distributed under the Creative Commons Attribution Non Commercial No Derivatives License (CC BY-NC-ND 4.0).

Unrestricted use, distribution, and reproduction of the original work are permitted for noncommercial purposes only, provided it is properly cited and its authors credited. No derivative of this work may be distributed.

### Keywords:

heat transfer; transonic; slot cooling; blade tips

### Citation:

Vieira J. A. C., Coull J., and Ireland P. (2024). Implementation of cooling slots at the pressure side rims of squealer tips. *Journal of the Global Power and Propulsion Society*, 8: 421–435.  
<https://doi.org/10.33737/jgpps/192452>

Joao Antonio Coelho Vieira<sup>1\*</sup>, John Coull<sup>2</sup>, Peter Ireland<sup>2</sup>

<sup>1</sup>Rolls-Royce, Moor Lane, Allenton, Derby DE24 9HY, United Kingdom

<sup>2</sup>University of Oxford, Wellington Square, Oxford OX1 2JD, United Kingdom

## Abstract

The blade tip is a particularly critical component of the high pressure turbine due to the hot overtip leakage gas being responsible for efficiency losses and thermal degradation, often limiting engine life. Squealer tip designs reduce the over-tip leakage mass flow, increasing efficiency, but the thin pressure side rims can be vulnerable to damage because of their large surface area and the difficulties of shielding them from hot overtip leakage flow. This paper considers a new approach to cooling these pressure side rims, by employing an inclined slot inside a recessed step. Compared to conventional cooling strategies, in which coolant is provided by multiple cylindrical holes, the slot feature improves cooling effectiveness by more than 50% in key regions of the pressure side rim, whilst also allowing for a substantial reduction in coolant mass flow. The concept design is developed and explored using Computational Fluid Dynamics (CFD) calculations, and the performance is validated experimentally in a linear cascade with representative Mach and Reynolds numbers.

## Introduction

A clearance gap must be maintained between the tips of rotating turbine blades and the stationary casing. For unshrouded designs, an Over-Tip Leakage (OTL) flow is driven through this gap by the pressure difference across the blade (Denton, 1993). The mixing generated by these OTL flows generates significant loss of aerodynamic efficiency throughout gas turbines. For this reason, squealer tips with thin external rims are often employed. As the OTL flow is constricted by both the pressure and suction side rims, such designs tend to reduce the leakage mass flow and thus the ensuing aerodynamic loss. In the High-Pressure (HP) turbine, the hot leakage flow can cause thermal degradation of the blade tip, e.g., via oxidation. This damage often constrains the overall engine life (Bunker, 2004). With the drive for ever-increasing thermal efficiency and turbine entry temperatures (Dutta et al., 2000), it is becoming increasingly difficult to sufficiently cool the HP blade tip, particularly at the pressure side rims and the thin Trailing Edge (TE) regions (Bunker, 2004). The aim of the current work is to substantially improve the cooling effectiveness in these regions.

In current gas turbines, the most common means to provide cooling to the PS rim is to use a series of discrete holes distributed along the external pressure surface of the blade. Numerous examples are given in Kwak and Ahn (2003), Bunker (2004), Ahn et al. (2005), Hofer and Arts (2009), Zhang et al. (2011), O'Dowd et al. (2013) and Saul et al. (2019). The conventional cooling approach shown in Figure 1a is used

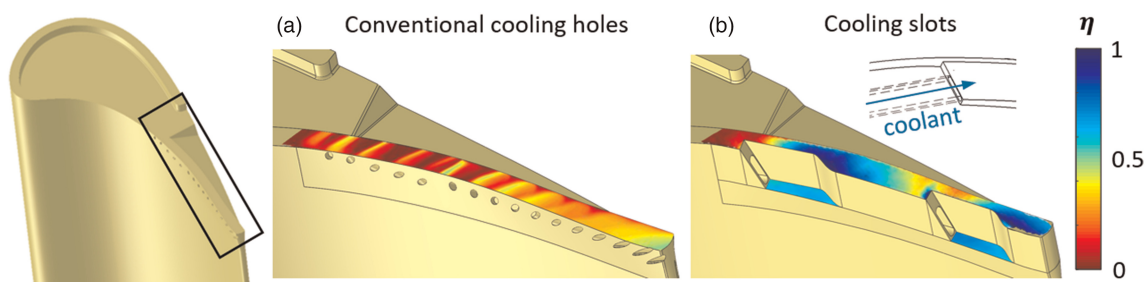


Figure 1. Experimental film cooling effectiveness contours overlapped over CAD renders of the tested high-pressure turbine tips.

as a baseline for the current study. This cooling configuration is applied to a squealer design with an opening on the aft. suction surface rim; however the findings are equally applicable to closed squealer, plain tip or winglet designs. As can be seen from the  $\eta$  measurements of cooling effectiveness (detailed below), the top of the rim is reasonably well-cooled at the blade trailing edge ( $\eta \sim 0.3$ ), but further upstream the cooling coverage is intermittent. This paper shows that the effectiveness can be significantly improved, allowing either an increase in engine life or an improvement in cycle efficiency via a reduction in cooling flows. This is achieved by developing a concept that employs a novel combination of slot cooling and tip shelves.

### Slot cooling

Compared to discrete film cooling holes, it has been long recognised that slots can achieve higher effectiveness on blade sections (e.g., (Cunha and Chyu, 2006)). In practice their use on aerofoil sections has been limited because of the stress limitations, but they have been used to cool aerofoil TE sections, which are highly vulnerable to damage. Yang and Hu (2012) experimentally examined the aerothermal performance of a rectangular slot geometry, focusing on the detailed measurement of the flow field via particle image velocimetry and correlating the identified features to the measured Film Cooling Effectiveness (FCE). Further work on TE slot cooling includes that of Niharika et al. (2016) and Wong et al. (2016).

Slot cooling has also been examined for cooling the interior cavity of squealer tips. Zhang et al. (2022) examined slots with radially-outward flow, distributed across the tip cavities in a cascade. While Zhang et al. (2021) introduced streamwise slots into their cavity by integrating them into ribs inside the cavity design. However, neither of these examples targeted the pressure surface rim.

### Squealer shelves

Another approach that has been seen in the patent literature, and some engines, is to place a small shelf into the exterior side of the PS rim and provide coolant using discrete, radially-aligned holes (Cherry et al., 2002; Leeke et al., 2003; Correia et al., 2008). In general, it is understood that a portion of the coolant tends to be trapped in the separation bubble generated as the OTL flow separates from the shelf edge, thus shielding the rim from hot flow. Further examples include the shelf at the TE of PS rim given in Crites et al. (2013). Another approach is shown in Lee et al. (1998), where a thin trench is cut into the tip of the squealer rim and fed with discrete cooling holes. The current study suggests that the inclined slots developed in this paper achieve significantly higher cooling effectiveness than these existing shelf designs.

### New concept: inclined slots with steps

The new cooling concept is shown in Figure 1b, and consists of a step on the Pressure Side (PS) rim of the blade tip with an inclined protrusion containing a cooling slot. With respect to previous designs, the key features to note are:

1. The design specifically targets the exterior of the squealer rim, rather than the cavity interior or blade TE.
2. The slot does not inject flow radially, but rather it is inclined in a largely streamwise direction. This factor is crucial to achieving a high area of coolant coverage. The streamwise momentum of the injected coolant causes coolant to follow along the length of the rim, rather than simply being drawn over the blade tip.
3. The slot is recessed into the blade by means of an inclined step cut into the squealer rim, rather than an axial shelf.

## Design parameters

Figure 2b shows an inclined slot applied to a squealer tip design. The cavity of this tip is open towards the trailing edge, but this feature is inconsequential for the slot performance. The slot exit is placed on an inclined step surface cut into the rim of the pressure surface, at around mid-chord in this example. A shelf cut into the pressure surface extends downstream of the slot and blends smoothly back into the blade. The following design parameters control the size and position of key features.

The slot and inclined step surface can be geometrically characterised as shown in Figure 2a. The distance from the bottom of the shelf ( $h$ ) and the offset from the external edge ( $d_{wall}$ ) were set to be 0.5% and 0.4% of axial chord ( $C_{ax}$ ) respectively to allow clearance for manufacturing. The width ( $w$ ) of the recessed step was set to 50% of the total rim width for all studied geometries. The length ( $l$ ) and diameter of the slot ( $d_n$ ) together control the slot aspect ratio and area, which is studied in detail in Section 3.2. For fixed mass flow, reducing slot area increases the Blowing Ratio (BR), thus increasing the streamwise momentum and spread of the coolant. Meanwhile, the higher flow gradients cause more mixing and effectiveness reduces more rapidly. Similar trade-offs are observed for fixed geometry with varying coolant flow rate.

The shelf length and height can be parametrized by three variables (Figure 2b). Longer shelf lengths ( $L$ ) require greater modification of the rim geometry, but can improve manufacturability by improving drill access for the slot. The depth ( $d$ ) sets the position of the slot in the spanwise direction. Together with the slot parameters,  $d$  sets the spanwise position of the slot and thus controls the coolant trajectory. The distance ( $d_{TE}$ ) controls the streamwise position of the shelf and slot.

The coolant ejection direction of the slot (Figure 2c) is defined by two angles: the vertical angle between the inclined surface and the shelf ( $\alpha$ ) and the pitch angle into the blade ( $\beta$ ). Of the two,  $\alpha$  has the largest impact on performance, since it defines the angle at which the coolant flow approaches the rim (see Section 3.3). Optimal coverage occurs at low values of  $\alpha$  and  $\beta$ , such that the coolant is injected along the streamwise direction of the PS rim. These angles will also be limited by manufacturing constraints.

## Nominal slot behaviour

Figure 3 shows a CFD prediction of the flow from a single slot at a tip gap size of 1.15% g/S - where the tip gap ( $g$ ) is normalised by the blade span ( $S$ ) - and a non-dimensionalised mass flow rate ( $\dot{m}_R$ ) of 45% (i.e., 45% of the baseline conventional design). In general, the coolant ejected from the inclined slot has a much higher streamwise momentum than the local mainstream flow, which tends to pass almost straight over the tip at this location. As a result, the coolant tends to propagate along the tip, cooling a larger area.

It is seen that most of the coolant follows the ejection direction of the slot for some distance, before being drawn over the top of the PS rim (pink streamlines in the figure). This behaviour provides relatively high  $\eta$  values for a section of the rim roughly equal to the shelf length in this case. After the high effectiveness region, the strong OTL flow causes the coolant to dissipate, which results in relatively low film effectiveness downstream of the shelf. In addition, Figure 3 also demonstrates that a portion of the coolant flow seeps into the separation region created by the shelf, where it propagates along the pressure surface to the blade trailing edge (blue streamlines).

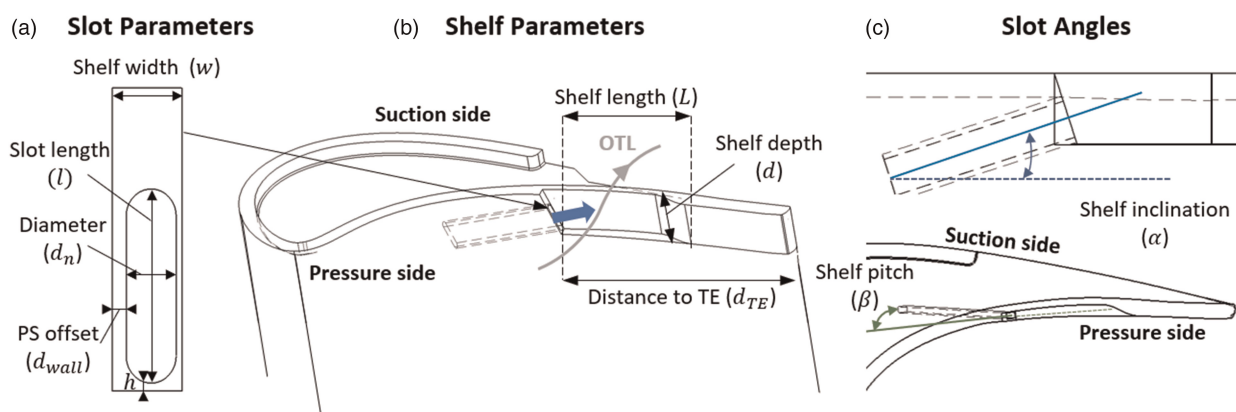


Figure 2. Schematic of the dedicated pressure side rim cooling slot depicting the parametrisation of its main features: a recessed PS shelf and an inclined cooling slot.

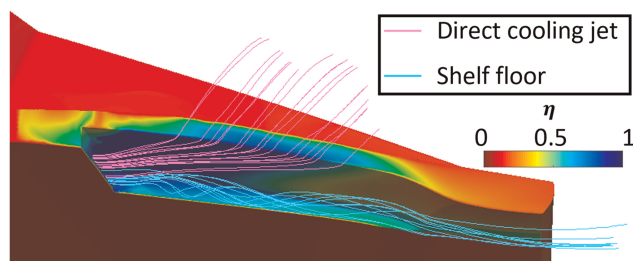


Figure 3. Film cooling effectiveness contour of the single cooling slot geometry at nominal conditions with superimposed streamlines showing the two modes of coolant propagation.

## Paper aims and approach

The key aims of this paper are to develop the inclined slot concept, to understand the flow behaviour and to quantify its performance compared to conventional cooling designs.

To this end, Computational Fluid Dynamics (CFD) simulations are used to rapidly explore the design space and understand the sensitivities. The most promising designs were then tested experimentally on a transonic cascade representative of HP turbines, which demonstrates the significant improvement in cooling effectiveness.

The paper is organised as follows: Section 2 describes the CFD procedure, including the detailing of a mesh sensitivity study and the film cooling effectiveness calculation methodology. Section 3 details the CFD studies of the design space, whilst the validation experiments are presented in Section 4. The data are complemented in Section 5 by simulating additional engine-representative conditions.

## Computation design study

The test vehicle for examining the slot concept is the High Speed Linear Cascade (HSLC) rig, designed to evaluate the aerothermal performance of HP turbine blade tips (described later in Section 4.1). The CFD calculations are largely performed at the experimental conditions, with the exception of the additional calculations described in Section 5, which examine in-engine effects that cannot be physically modelled in the cascade, namely coolant density and the relative motion of the casing.

## Meshing and CFD

To model the cascade, a single periodic passage is simulated, with the inlet plane located two axial chords upstream of the blade Leading Edge (LE) and the outlet one axial chord downstream of the TE. A distribution of total pressure matching the cascade is specified at the inlet, together with constant total temperature and flow angle. The slot inlet feed is setup as a constant mass inflow, with fixed inlet angles and temperature. A constant static pressure is specified at the outlet. The hub, casing and the entirety of the blade are no-slip walls.

An unstructured mesh was generated using BoxerMesh, combining an octree freestream mesh with body-fitted viscous layers (Figure 4). Surface  $y^+$  values in the order of 0.5 were obtained for the entirety of the tip region. The mesh resolution at the tip is particularly high, with a refinement focus in the region downstream of the slot, which is the principal area of interest for the study. Total mesh size depends on the geometry, but is typically between 20 and 22 million nodes, in accordance to the mesh independence study presented below (Section 2.3).

Reynolds-Averaged-Navier-Stokes (RANS) calculations are performed using the Rolls-Royce in-house Hydra solver (Moinier, 1999). Spatial discretisation is performed with a 2nd order upwind edge-based finite volume method and time stepping employs a 5th order Runge-Kutta explicit scheme with Jacobi preconditioning. The turbulence model used in this study was  $k-\omega$  with Shear-Stress Transport scheme (Menter, 1994).

## Film cooling effectiveness calculation and associated performance metrics

A two-temperature approach was used to calculate the surface FCE of the CFD simulations, by comparing the surface temperature data of two simulations with coolant temperatures set 10 degrees apart:

$$\eta = \frac{T_{\text{ref}} - T_{\text{test}}}{T_g - T_c} \quad (1)$$

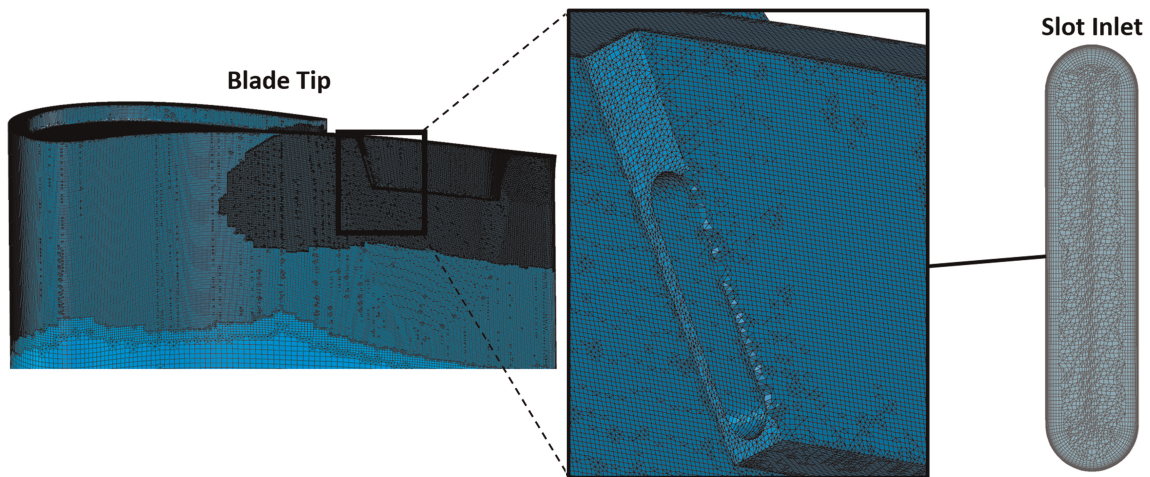


Figure 4. Details of the numerical mesh for an example inclined slot geometry.

where  $T_g$  and  $T_c$  are the total temperatures of the mainstream (285 K) and of the coolant (275 K), respectively. The blade tip surface temperatures of the “reference” case ( $T_{ref}$ ) represent the nominal condition with the coolant inlet set to the same temperature as the mainstream (285 K), whilst the temperatures in the cooled “test” simulation ( $T_{test}$ ) portray the impact of the coolant stream, with the coolant set to 275 K.

While the pointwise  $\eta$  over the surface of the tips is an useful comparison metric on its own, it is also useful to establish the following integrated parameters:

- $\overline{\eta}_{top}$ : spatial-averaged  $\eta$  over the top surface of the PS rim, between 60% and 100% axial chord ( $C_{ax}$ ).
- $\overline{\eta}_{side}$ : spatial-averaged  $\eta$  over the side surface of the PS rim. Averaging region is, again, between 60% and 100%  $C_{ax}$  in the axial direction and between 90% and 100% of blade span.
- $\overline{\eta}_{av}$ : area-based weighted average of  $\overline{\eta}_{top}$  and  $\overline{\eta}_{side}$ .

Figure 5 color-codes top and side averaging regions on an example geometry. These are the key regions of the PS rim that the dedicated slot concept aims to cool, in lieu of conventional cooling holes.

### Mesh sensitivity

Mesh independence was evaluated on a single case. A total of five meshes with identical mesh refinement settings with increasing grid density were examined, ranging from 7.4 to 39 million nodes. Grid sensitivity is assessed first by considering area-averaged FCE over the two regions denoted in Figure 5, and second by considering local FCE at four points downstream of the slot exit. The data in Figure 6 evidences that suitable convergence occurs at mesh sizes of 20 million nodes, where the variation in global FCE is only 0.25% compared to the case with the highest mesh density. Expectedly, larger variations are observed in the localised FCE data present in high-dissipation regions, which is the case for points 2, 3 and 4. Nevertheless, the  $\eta$  values at these points converge

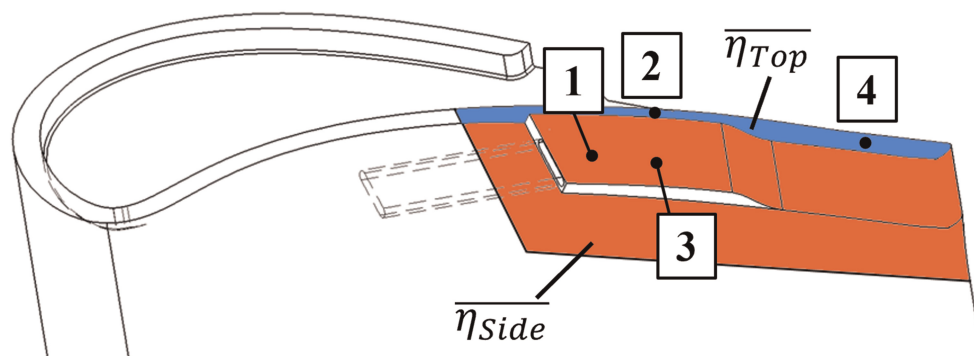


Figure 5. Averaging regions for the cooling evaluation parameters. Numbered positions are the probing points implemented in the mesh independence study.

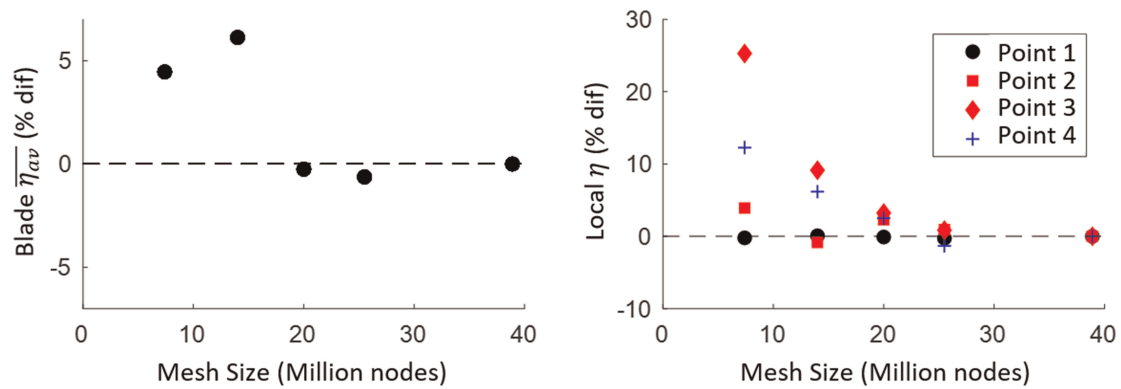


Figure 6. Percentage deviation of the mesh independence criteria from the values obtained at the highest density grid, plotted against number of nodes.

convincingly with the increase of mesh density. Accordingly, the meshes for all the CFD cases in this publication were generated with the same refinement settings as the 20 million node grid.

### Exploring the design space

The performance of the inclined slot concept is first studied in CFD. In this chapter the overall performance of some key designs are assessed, before sensitivities to design parameters and dual-slot configurations are explored. The range of design parameters for each case are given in Table 1, which will be referenced throughout this section.

### Overall performance of the studied geometries

The overall performance of various slot designs are compared to the conventional cooling design from Figure 1a. Figure 7 charts the average film effectiveness in the region-of-interest:  $\overline{\eta}_{av}$  (see Section 2.2), against the non-dimensionalised mass flow rate for cases at 1.15% g/S tip clearance. The diamond marker is the baseline reference value, the circles show single slot configurations, and the dashed lines link cases that were examined at multiple coolant mass flow rates. The square symbols indicate the dual slot design, discussed in detail in Section 3.4. The conventional baseline tip is on the bottom-right, having the lowest  $\overline{\eta}_{av}$  value (0.11) and the highest

Table 1. Parameters of the geometries involved in the study of the inclined slot concept.

	Cases	$l/C_{ax}$	$\alpha$	$\beta$	$d_n/C_{ax}$	$L/C_{ax}$	$d/C_{ax}$	$w/C_{ax}$	$d_{TE}/C_{ax}$
Slot Area Study	Smaller slot area	5.5%	18°	8°	1.6%	36.0%	12.2%	2.0%	50.0%
	Nominal case	8.3%							
	Larger slot area	11.1%							
$\alpha$ Study	Angle $\alpha$ case 1	8.3%	4°	8°	1.6%	36.0%	12.2%	2.0%	50.0%
	Angle $\alpha$ case 2		30°						
	Angle $\alpha$ case 3		45°						
$\beta$ Study	Angle $\beta$ case 1	8.3%	18°	0°	1.6%	36.0%	12.2%	2.0%	50.0%
	Angle $\beta$ case 2			16°					
Double Slot Study	{ Fwr. Slot Aft. Slot }	8.3%	18°	8°	1.6%	20.0%	12.2%	2.0%	{ 62% 24% }

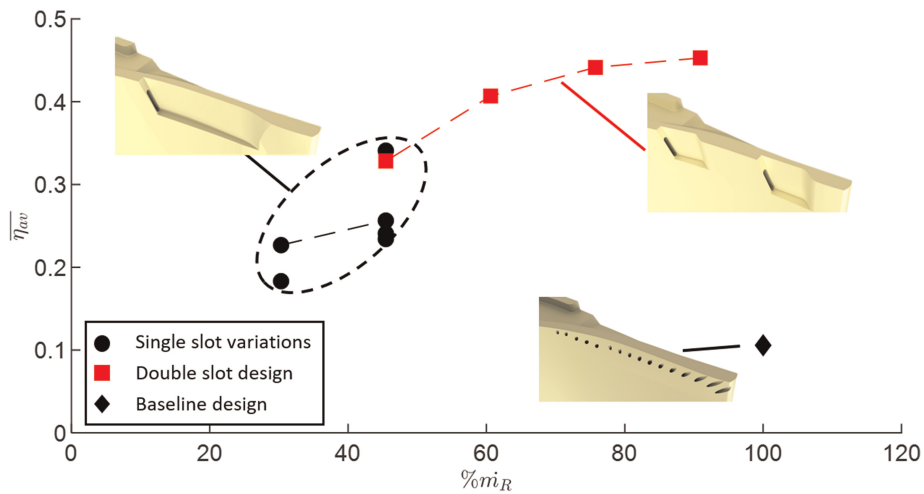


Figure 7. Average film cooling effectiveness ( $\overline{\eta}_{av}$ ) plotted against total coolant mass flow. Single slot geometries are shown as circles, dual slot design as squares and the baseline tip as a diamond.

coolant expenditure. On the left, the range of single slot variants are distributed between  $\overline{\eta}_{av}$  values of 0.18 and 0.34. The dual slot geometry matches the highest performing single slot cases at  $\dot{m}_R = 45\%$  and then proceeds to significantly improve upon that as the coolant mass flow increases, with the  $\dot{m}_R = 91\%$  case having the highest  $\overline{\eta}_{av}$  of the studied cases, at a value of 0.45.

The following two subsections will examine the impact of key slot design parameters on the cooling performance, arranged from highest to lowest relative importance: slot flow area (3.2) and slot angles (3.3). Dual slot designs are then discussed in Section 3.4. Table 1 shows the parametrisation of the test geometries for each study.

### Sensitivity to slot flow area

The first case study is that of the slot coolant ejection area. The slot flow area is defined by the slot length ( $l$ ) and nominal diameter ( $d_n$ ). As shown in the first row of Table 1,  $d_n$  was kept constant at  $1.6\% C_{ax}$ , while  $l$  was varied between  $5.5$  and  $11.1\% C_{ax}$  to give a  $\pm 33\%$  variation in area from the nominal slot design. The three cases were simulated at a tip gap size of  $1.15\% g/S$ .

Figure 8 charts the average effectiveness values on the top and side surfaces against the coolant ejection area. Black markers refer to  $\overline{\eta}_{top}$  and red markers to  $\overline{\eta}_{side}$ , while the diamond markers are reference values for the baseline tip. The relationship between coolant coverage and slot BR is evidenced in the slot data where it is seen that both averages peak at nominal slot flow area ( $A_i = 1$ ).

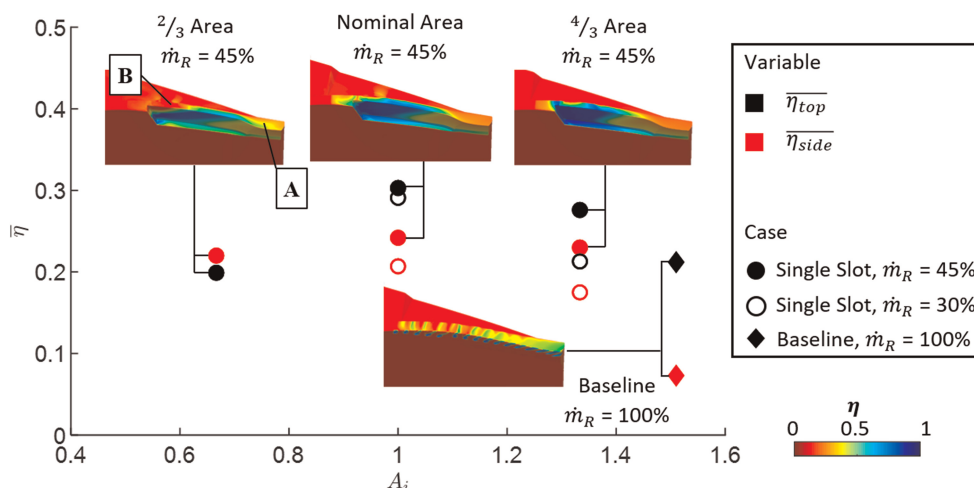


Figure 8. Area-averaged  $\eta_{top}$  and  $\eta_{side}$  for the cases with varying slot flow area ( $A_i$ ).

Slot blowing ratio is defined as:

$$BR = \frac{\rho_c V_c}{\rho_m V_m} \quad (2)$$

Where the numerator refers to the velocity and density of the coolant, whilst the denominator refers to the mainstream gas. Thus - for fixed mass flow rates - decreasing the slot area increases jet velocity, causing the slot BR to increase, whilst the reverse occurs when the area is increased. The effects of decreasing slot area on the cooling distribution can be seen in the  $2/3 A_i$  case (leftmost insert plot). The smaller area increases the blowing ratio of the slot, causing the coolant to be projected further along the PS rim, at the detriment of effectiveness in the near-slot region. This change leads to an increase of  $\eta_{top}$  in the latter 10%  $C_{ax}$  of the rim (label A in the figure), but significantly lowers the values in the 60 to 85%  $C_{ax}$  region (label B). In addition, the higher velocity jet undergoes greater dissipation, lowering average  $\eta$  values. A similar effect occurs on the side of the rim, where this case achieves slightly more coverage after the 80%  $C_{ax}$  point, while having lower upstream values.

Inversely, the larger slot flow area case (rightmost insert plot) causes a decrease in slot BR, shifting the coolant coverage and associated peak  $\eta$  values upstream. This factor leads to a large improvement in near-slot  $\eta_{top}$ , but penalises  $\eta_{side}$  on the latter 20%  $C_{ax}$  of the rim. A similar effect is observed when BR is changed by varying mass flow rate for a given design (clear circle markers in Figure 8), which highlights the dependency of the coolant distribution on slot blowing ratio. It is also seen that the nominal flow area slot case is less affected by the decrease in coolant mass flow rate than the larger area case, which underwent a reduction of  $\sim 30\%$  in both performance metrics. This difference is largely due to the slot BR in each of the cases, which at nominal slot area results in jets that have a higher resilience to the change in coolant mass flow.

Overall, compared to the baseline tip (diamond markers in the figure), it is shown that the single slot geometries greatly outperform the reference conventional design in both  $\overline{\eta_{top}}$  and  $\overline{\eta_{side}}$  for most of the examined region, with the conventional tip only achieving superior  $\eta_{top}$  coverage at the last 10%  $C_{ax}$  of the rim. Average values for the nominal flow area case show a 44% improvement over the reference for  $\overline{\eta_{top}}$  and of 250% for  $\overline{\eta_{side}}$ , with a coolant expenditure of less than half that of the reference case.

In summary, it is seen that the cooling performance of the dedicated slot geometry is highly dependent on slot blowing ratio, with the data suggesting that blowing ratio increases are less penalising to the overall performance than blowing ratio decreases. For this dedicated slot configuration, at the identified optimal conditions, there is an optimal area of coverage consisting of roughly 20%  $C_{ax}$  downstream of the slot. This area can be increased by increasing slot blowing ratio, at the cost of having more diffuse coolant. Alternatively, one can also increase the number of slot features along the rim, which maximises both coverage and performance. This hypothesis is explored in Section 3.4.

### Sensitivity to slot angles $\alpha$ and $\beta$

The orientation of the cooling slot in relation to the shelf plays an important role on jet direction and coolant propagation. This section details the study of the impact of the vertical angle  $\alpha$  and the pitchwise angle  $\beta$  (Figure 2c) on the cooling performance. In total, five variations to the baseline geometry were examined, three with incremental  $\alpha$  angles:  $4^\circ$ ,  $30^\circ$  and  $45^\circ$ ; and two with incremental  $\beta$  angles:  $0^\circ$  and  $16^\circ$ , as shown in the middle two rows of Table 1. The lower  $\alpha$  and upper  $\beta$  bounds of these distributions were established by the geometrical limitations of the underlying tip geometry, thus exploring the full range of allowable values. The nominal slot flow area case is also included as a sixth case, with the angles  $\alpha = 18^\circ$  and  $\beta = 8^\circ$ . All cases were simulated at a tip gap size of 1.15% g/S and a coolant mass flow of  $\dot{m}_R = 45\%$ .

It is immediately apparent from the datapoints in Figure 9a that lower  $\alpha$  angles improve: (1) the  $\eta$  magnitude on the top surface of the rim and (2) the overall coverage on the side surface. This increase in performance is expected, as lower  $\alpha$  angles improve the alignment of the cooling jet with the shelf, which allows the jet to more effectively fill the shelf and enhances the shielding of the coolant against the dissipative action of the OTL flow. Additionally, the larger amount of coolant inside the shelf is greatly beneficial to  $\eta_{side}$ , as it not only improves the coverage on the side rim surface inside the shelf, but also increases downstream propagation along the side of the blade (Figure 3). In overall terms, this behaviour results in an essentially linear decrease of  $\overline{\eta_{side}}$  with the angle  $\alpha$ , as is shown by the red circular markers in Figure 9.

The impact of  $\alpha$  on the top surface is more subtle. Black markers in the figure show that the most significant change occurs between the  $30^\circ$  and  $45^\circ$  cases, where the extreme slot inclinations cause the coolant to be mostly convected directly into the tip gap rather than propagating along the rim, considerably reducing coverage. Contrastingly, the two other  $\alpha$  cases are mostly identical, except for the near-slot region, with the difference

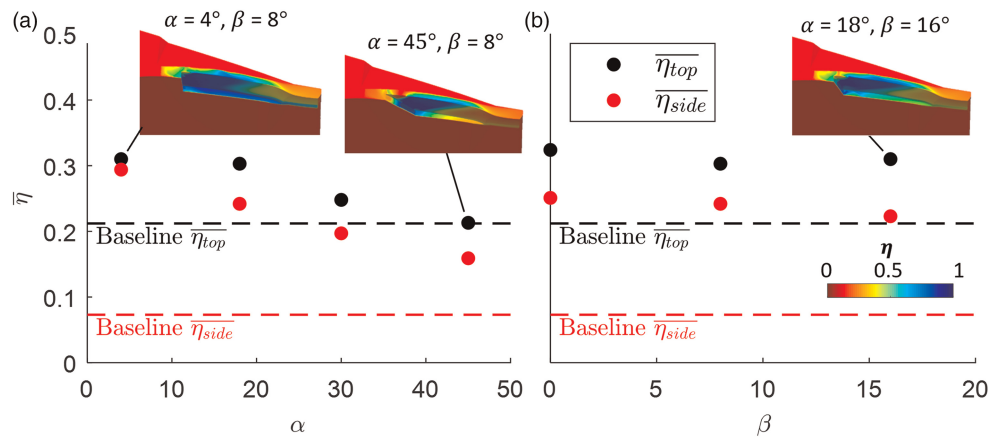


Figure 9. Area-averaged  $\eta_{top}$  and  $\eta_{side}$  for the cases with varying  $\alpha$  and  $\beta$  slot angles. Dashed lines are the reference values for the conventionally cooled baseline tip.

between the  $\alpha = 4^\circ$  and the  $\alpha = 18^\circ$  cases being just 2.3%, which implies that reducing  $\alpha$  below  $20^\circ$  has diminishing benefits on the coverage of the top of the rim.

Sensitivity to  $\beta$  is shown in Figure 9b. The pitchwise angle has an overall smaller impact on cooling performance compared to  $\alpha$ , partly due to the smaller feasible range of values (limited by blade thickness). Expectedly, the  $\beta = 0^\circ$  case achieves the highest performance values, as this is the condition in which the coolant stream is parallel to the shelf surface and, thus, can more easily propagate along the rim surfaces. As the  $\beta$  angle increases, the coolant flow is gradually redirected away from the blade and into the ascending OTL flow, decreasing the amount of coolant available inside the shelf. On the side surface, this change results in a consistent, albeit small, reduction of  $\overline{\eta}_{side}$ , with the  $\beta = 16^\circ$  having an overall value 11% lower than the  $\beta = 0^\circ$  case. In contrast, the only major difference at the top rim surface is the near-slot region in the  $\beta = 0^\circ$  case, resulting in a 7% increase over the nominal conditions ( $\beta = 8^\circ$ ), which performs almost identically to the  $\beta = 16^\circ$  case. Designs with higher  $\beta$  values would be expected to have worse cooling performance, but these are impractical unless thicker blade profiles were to be adopted.

In summary, it is apparent from these two studies that the dedicated PS slot geometry functions optimally at low slot  $\alpha$  and  $\beta$  angles, so that the cooling jet is directed approximately parallel to the PS rim.

## Dual slots

The single slot designs achieved promising results in relation to conventional cooling schemes and were shown to be capable of cooling a region of up to 20%  $C_{ax}$  downstream of the slot. As depicted in Figures 8 and 9, this effective range resulted in undesirably low coolant coverage on the last 10%  $C_{ax}$  section of the PS rim. Increasing blowing ratio can increase coverage far downstream of the slot, but this results in greater near-field mixing, leading to a substantial reduction in overall cooling performance.

A dual slot configuration can be adopted to achieve greater coverage with high FCE. As shown in Figure 7, the design consists of two smaller shelves - with lengths of 20%  $C_{ax}$  - distributed along the TE of the PS rim. Location-wise, the  $d_{TE}$  of the fwr. shelf is 62%  $C_{ax}$ , while for the aft. shelf it is 24%  $C_{ax}$ . All other parameters of the two features are the same as those of the single slot design with nominal area (last row in Table 1). This dual slot geometry was simulated at four coolant mass flows, split equally between the two cooling orifices: from  $\dot{m}_R = 45\%$  to  $\dot{m}_R = 91\%$  total coolant feed.

The  $\eta$  distributions are shown in the insert plots of Figure 10, a stark contrast exists between the dual slot and the single slot results (shown in Figures 8 and 9). Particularly, there is a more complete cooling of the top of the rim, where the coverage provided by the fwr. slot is succeeded by that of the aft. slot, resulting in a substantially more consistent coverage of the target region. It should be noted that a low  $\eta$  patch is present between the shelves in the cases with lower  $\dot{m}_R$ , which is completely eliminated in the higher  $\dot{m}_R$  cases, as demonstrated in the right-hand insert plot in Figure 10.

In regards to the general trends, data shows that increasing  $\dot{m}_R$  is beneficial for the size and concentration of the coolant distribution on the downstream tip surfaces, causing a consistent increase in  $\overline{\eta}_{top}$  and  $\overline{\eta}_{side}$  up to  $\dot{m}_R = 76\%$ . However, little performance gains are present between the  $\dot{m}_R = 76\%$  and  $\dot{m}_R = 91\%$  cases, with an increase in performance metrics of only 2.5%, at the cost of 20% added coolant. These factors evidence a

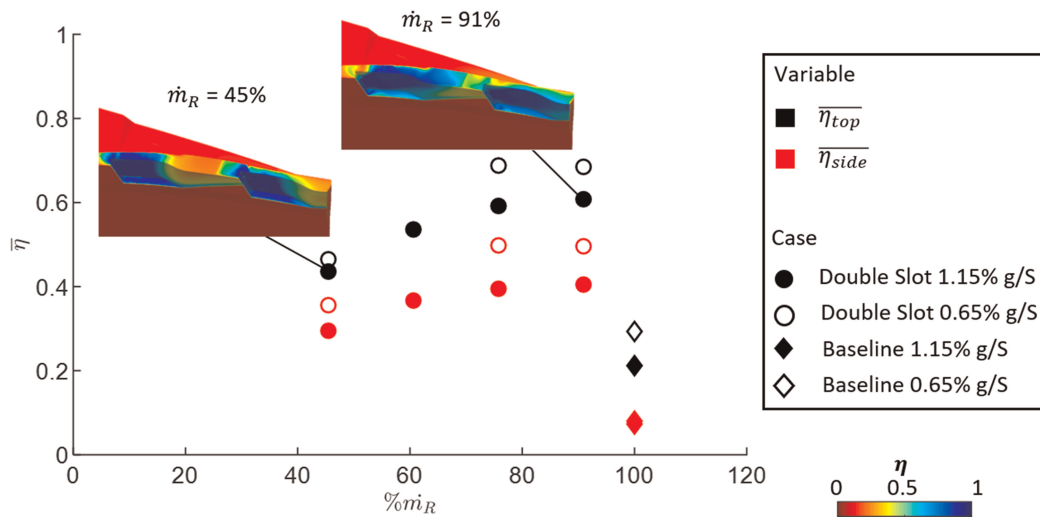


Figure 10. Area-averaged  $\eta_{top}$  and  $\eta_{side}$  for the double slot cases with varying coolant mass flow rate and tip gap size. Note that the y-axis limits differ from previous  $\bar{\eta}$  plots.

performance plateau of the dedicated PS slots, with the limiting coolant mass flow rate at the tested conditions being roughly  $\dot{m}_R = 45\%$  per slot.

In comparison to the reference values of the baseline tip (diamond markers in the figure), the double slot  $\dot{m}_R = 91\%$  case further develops on the benefits of the single slot configurations, achieving improvements of 185% and 455% over the  $\bar{\eta}_{top}$  and  $\bar{\eta}_{side}$  of the baseline, respectively, whilst using 9% less coolant. Moreover, since the performance of the  $\dot{m}_R = 76\%$  case is similar to that of the  $\dot{m}_R = 91\%$  case, these large improvements are achievable whilst saving roughly 25% of the coolant budget.

The impact of tip clearance was also examined in this study, with the clear circle markers representing the cases with smaller tip clearance (0.65% g/S). The data for the small tip gap cases show a substantial increase of  $\bar{\eta}_{top}$  and  $\bar{\eta}_{side}$ , likely due to the smaller OTL mass flow causing less dissipation of the cooling jets and increasing overall coolant residency time. Thus, it is seen that the tip clearance reduction has a positive impact on the cooling performance of the dedicated PS slot over both rim surfaces.

In summary, the dual dedicated PS slot geometry demonstrates a substantial increase in cooling effectiveness over the conventional cooling schemes. The following section presents an experimental validation of this concept.

## Experimental demonstration of the dual slot design

### High speed linear cascade

The Oxford HSLC is a 5-blade cascade with variable tip gap, which operates as a blowdown facility with around 90 s of run time (Vieira et al., 2021). The experiments are run at transonic exit Mach number (0.99) and a Reynolds number based on true chord and exit conditions of  $1.24 \times 10^6$ . Further details can be found in Zhang et al. (2011) and O'Dowd et al. (2013).

Film cooling is delivered to the blade tips using dedicated cooling feeds, while cooling effectiveness distributions are measured using dual-component Pressure Sensitive Paint (PSP). This optical measurement method employs a mass transfer analogy to obtain adiabatic film cooling effectiveness, with the calculation evaluating the phosphorescent excitation of the PSP coat applied to the test pieces, the emissivity of which is dependent on the local partial pressure of Oxygen. This property is exploited to calculate local partial pressures using a filtered color-corrected camera (Han and Rallabandi, 2010). For each measurement, ambient temperature Air and Nitrogen are sequentially used as coolant to generate a comparative evaluation, in which Nitrogen functions as an effective tracer gas for the distribution of coolant over the surface of the blade. Dual-component PSP includes a second, temperature-dependent paint that allows corrections for temperature variation, leading to greater accuracy in the calculated effectiveness. Linear perturbation analysis demonstrates that the experimental uncertainties depend on the signal level, giving local uncertainties of approximately  $\pm 0.045$  for  $\eta < 0.2$  and  $\pm 0.015$  for  $0.2 < \eta < 1.0$ , at a 95% confidence level.

Though not the focus of this paper, aerodynamic measurements are also performed  $0.5 C_{ax}$  downstream of the cascade trailing edge using a 4-hole probe with 1.2 mm head diameter. Traverses consist of a grid of 26 pitchwise locations by 10 spanwise locations. Total pitchwise length is one blade pitch, while spanwise length is 25% of blade span.

## Experimental results

The film cooling effectiveness of the dual slot design was measured on the HSLC via a test tip manufactured with stereolithography additive manufacturing using ABS plastic, with the rims edges and cooling orifices being machined to match geometrical specifications. Test conditions for this geometry were the smaller tip gap setting (0.65% g/S) and the four coolant mass flow rates from the CFD study, which range from  $\dot{m}_R = 45\%$  to  $\dot{m}_R = 91\%$ , with the coolant being equally distributed between the two slots. Results are shown in Figure 11. In addition, some optimisation of the coolant balance between the two slots was attempted, with the most successful case being a  $\dot{m}_R = 76\%$  configuration with a 3:2 split, resulting on 60% of the coolant being routed to the fwd. slot and the remaining 40% to the aft. slot (clear circle marker).

The  $\eta$  insert plots presented in the figure demonstrate that the excellent coolant coverage of the top rim surface generated by the dual slot design is successfully replicated in an experimental setting, corroborating the performance predicted in the CFD study. Impressively, the coolant distribution over the target TE portion of the rim is already exemplary in the  $\dot{m}_R = 45\%$  case (left insert plot) and improves further as additional coolant is added, with near perfect coverage of the rim being achieved in the  $\dot{m}_R = 91\%$  case (right insert plot).

In comparison to the experimental  $\overline{\eta}_{top}$  value for the baseline tip at small tip gap, the dual slot design is shown to comfortably surpass the performance of the conventional cooling scheme throughout the trailing edge region of the rim, representing a coolant savings of 9% in the  $\dot{m}_R = 91\%$  case, while improving  $\overline{\eta}_{top}$  by 46%. Optimising the split of coolant flow between the two slots maintained performance while saving approximately a quarter of the coolant mass flow rate. Furthermore, the experimental data do not include the improvements on the side of the rim, where the CFD predicts that the double slot configuration should greatly outperform the conventional cooling scheme. Thus, it is expected that the overall cooling advantage is greater than the value quoted above. The aerodynamic loss of the dual slot, as measured by the 4-hole probe, showed no significant differences in performance to that of the baseline tip.

In comparison to the CFD data from Section 3.4, the dual slot cases exhibited a  $\overline{\eta}_{top}$  progression that is very similar to that predicted by the simulations. For reference, the red square markers in Figure 11 denote the CFD cases at the same tip clearance as the experimental data (0.65% g/S). As can be seen, CFD overpredicted the experimental effectiveness for the two higher  $\dot{m}_R$  cases by approximately 20%, which shows a significant magnitude mismatch, but still represents a relatively close agreement for RANS simulations of film cooling effectiveness performance.

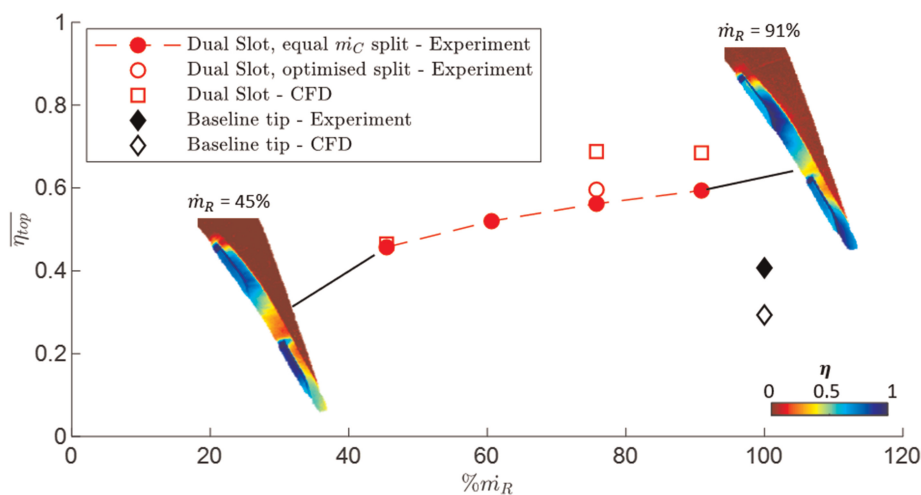


Figure 11. Plot of  $\overline{\eta}_{top}$  experimental averages against coolant mass flow rate for the double slot and baseline tip geometries at small tip gap.

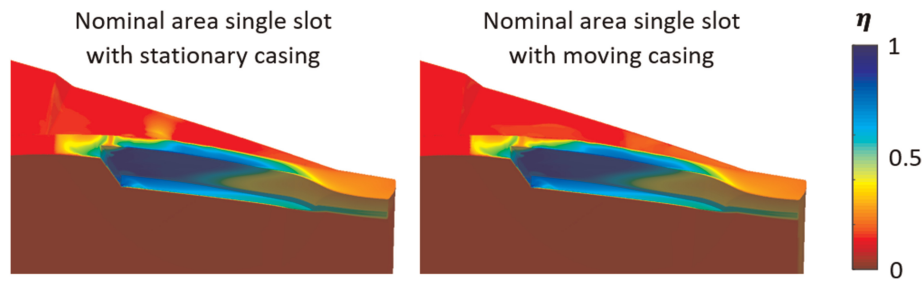


Figure 12. Film cooling effectiveness contours for the single slot geometry with flow nominal area and 1.15% g/S tip clearance. Case on the left has stationary casing, while the case on the right is setup with engine-representative casing motion.

## Sensitivity to real-engine effects

### Relative casing motion

The previously described simulations and experiments were realised in a purely stationary frame. To address the impact of rotor rotation on the cooling performance of the slot features, the baseline version of the single slot geometry from Section 1.5 was simulated with engine-representative casing motion. All other aspects of the setup are identical to those described in Section 2.1. The  $\eta$  distributions with and without casing motion are shown in Figure 12, and show only very minor differences. Both  $\overline{\eta}_{top}$  and  $\overline{\eta}_{side}$  are within 1% for the two cases. This resilience to the scraping flow is consistent with similar calculations performed by Virdi et al. (2015), Ma et al. (2017) and Saul et al. (2019), as well as the model of Dambach et al. (1999). The OTL flow at the rear of the rims is dominated by pressure differentials and not casing motion, thus the cascade setup is representative of the engine.

### Coolant density

One limitation of the experimental setup is that the coolant-to-mainstream density ratio is approximately unity ( $\rho_{ratio} = 1$ ). For the dual-slot geometry, CFD predictions in Figure 13 show the sensitivity to density ratio: Figure 13a shows the effectiveness for unity density ratio. For higher coolant density and matching mass flow rate, Figure 13b shows that the near-slot effectiveness remains very high but the downstream effectiveness reduces. This effect is caused by a reduction in the blowing ratio, as per the results in Figure 8. Without changing the slot geometry, the original performance can be restored by increasing the mass flow rate by approximately 30% (Figure 13c), so that the cooling jet Mach numbers match the unity-density case in 13.a. In practice, one can achieve similar performance by reducing the slot width  $d_n$  to preserve blowing ratio while maintaining the mass flow rate.

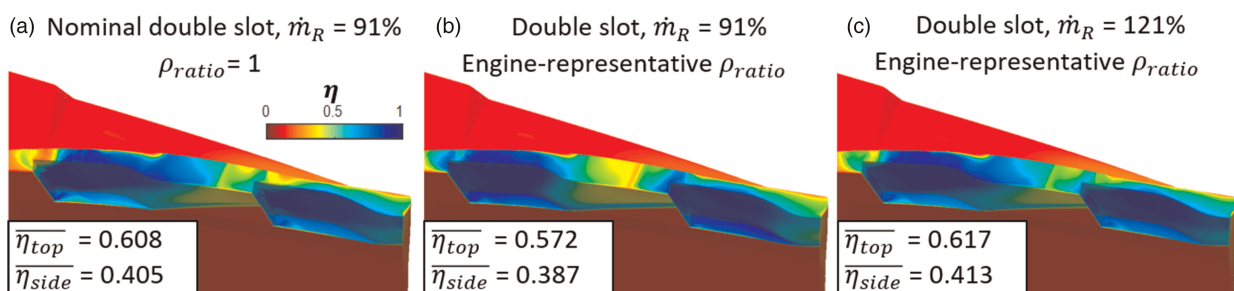


Figure 13. Film cooling effectiveness contours for the double slot geometry. On the left, nominal case discussed in Sections 3.4 and 4. On the middle, case with the same coolant mass flow rate but with an engine-representative density ratio. On the right, case with engine-representative density ratio and matching jet Mach number to that of the nominal condition.

## Conclusions

---

This paper has demonstrated the potential benefits of the inclined slot cooling concept for cooling blade tips. Numerical simulations explored the design space and the most promising geometry was experimentally demonstrated in a cascade. The key conclusions are as follows:

- It was demonstrated, both experimentally and numerically, that the inclined slot concept has the potential to greatly improve tip cooling of the pressure side rim, an often at-risk region of the tip.
- As per conventional cooling holes, the inclined slot performance is dependent on the blowing ratio. The behaviour can be largely understood by considering the injected streamwise momentum. Low blowing ratios lead to higher coolant concentrations near the slot, but with little streamwise propagation. Conversely, higher blowing ratios cause the coolant to propagate over a longer distance, enhancing downstream coverage. However, coolant concentration in the near-slot region reduces due to enhanced mixing with the mainstream flow. For a balanced blowing ratio, the slot designs can achieve high levels of coolant coverage over a distance of around 20%  $C_{ax}$  downstream of the slot.
- Higher effectiveness is achieved when the coolant injection is aligned with the pressure side rim in the streamwise direction, enabling the jets to more easily propagate along the rim surfaces.
- The double slot configuration maximises coolant concentration and coverage. The two slots can be adjusted to work in tandem at their respective optimal ranges. This configuration achieved continuous high coolant density over the pressure side rim, greatly outperforming conventional cooling strategies.
- Experimental cascade data corroborate the numerical studies. Compared to conventional cooling designs, the double slot geometry achieved an effectiveness improvement of 45% on the rim tips, whilst using 25% less coolant.
- Further computations show that the inclined slot design should have high performance in real turbine conditions. Relative casing motion has negligible impact on performance because the local over-tip flow is pressure dominated. In contrast, matching coolant-to-mainstream density ratio reduces the injected momentum of the coolant jet, which can be corrected for by reducing the slot area to increase the injected velocity.

## Nomenclature

---

### Abbreviations

BR	Blowing Ratio
dif	Difference
FCE	Film Cooling Effectiveness
HP	High-Pressure
LE	Leading Edge
OTL	Overtip Leakage
PS	Pressure Side
SS	Suction Side
TE	Trailing Edge

### Symbols

$A_i$	Initial Area ( $m^2$ )
$C_{ax}$	Axial Chord (m)
$d$	Distance or Shelf Depth (m)
$d_n$	Slot Nominal Diameter (m)
$g$	Tip Gap (m)
$h$	Shelf bottom offset (m)
$l$	Slot Length (m)
$L$	Shelf Length (m)
$\dot{m}_R$	Non-dimensionalised Coolant Mass Flow Rate
$S$	Blade Span (m)
$T$	Temperature (K)
$V$	Velocity (m/s)

$w$	Shelf Width (m)
$\alpha$	Shelf Inclination
$\beta$	Shelf Pitch
$\eta$	Film Cooling Effectiveness
$\rho$	Density ( $\text{kg/m}^3$ )

## Subscripts

$av$	Area-Average
$c$	Coolant
$g$	Gas
$m$	Mainstream
test	Test or Baseline
top	Top Surface
ref	Reference
side	Side Surface
wall	Wall

## Funding sources

This worked was funded by Innovate UK iCore Impact Acceleration Scheme.

## Competing interests

Dr. Joao Antonio Coelho Vieira declares that he has no conflict of interest. Prof. John Coull declares that he has no conflict of interest. Prof. Peter Ireland declares that he has no conflict of interest.

## References

- Ahn J., Mhetras S., and Han J. (2005). Film-cooling effectiveness on a gas turbine blade tip using pressure-sensitive paint. *Journal of Turbomachinery*. 127: 521–530. <https://doi.org/10.1115/1.1909208>.
- Bunker R. (2004). Blade tip heat transfer and cooling techniques, von Karman Institute for Fluid Dynamics, Lecture Series 2004.
- Cherry D., Lee C., Prakash C., Wadia A., Keith B., and Brassfield S. (2002). Turbine blade having angled squealer tip. U.S. Patent 6,672,829.
- Correia V., Manning R., and Reddy B. (2008). Turbine blades and turbine blade cooling systems and methods. U.S. Patent 20,080,131,278.
- Crites C., Morris C., and Halfmann S. (2013). Ep 2 639 405 a1'. EU Patent EP 2 639 405 A1.
- Cunha F. and Chyu K. (2006). Trailing-edge cooling for gas turbines. *Journal of Propulsion and Power*. 22: 286–300. <https://doi.org/10.2514/1.20898>.
- Dambach R., Hodson H. P., and Huntsman I. (1999). An experimental study of tip clearance flow in a radial inflow turbine. *Journal of Turbomachinery*. 121 (4): 644–650. <https://doi.org/10.1115/1.2836716>.
- Denton J. (1993). Loss mechanisms in turbomachines. *Journal of Turbomachinery*. 115: 621–656.
- Dutta S., Ekkad S., and Han J. (2000). *Gas Turbine Heat Transfer and Cooling Technology*. Florida: CRC Press.
- Han J. and Rallabandi A. (2010). Turbine blade film cooling using PSP technique. *frontiers in heat and mass transfer. Frontiers in Heat and Mass Transfer*. 130: 021002. <https://doi.org/10.1115/1.2776949>.
- Hofer T. and Arts T. (2009). Aerodynamic investigation of the tip leakage flow for blades with different tip squealer geometries at transonic conditions. *Proceedings of the ASME Turbo Expo*. 7: 1051–1061. <https://doi.org/10.1115/GT2009-59909>.
- Kwak J. and Ahn J. (2003). Heat transfer coefficients and film cooling effectiveness on the squealer tip of a gas turbine blade. *Journal of Turbomachinery*. 125: 648–657. <https://doi.org/10.1115/1.1622712>.
- Lee C., Branch G., and Isburgh A. (1998). Slot cooled blade tip. U.S. Patent 573,310,2A.
- Leeke L., Keith S., Rae R., Lenahan D., Harris D., and Frey D. (2003). Ramped tip shelf blade. U.S. Patent 20,030,059,304.
- Ma H., Zhang Q., He L., Wang Z., and Wang L. (2017). Cooling injection effect on a transonic squealer tip—part i: Experimental heat transfer results and cfd validation. *Journal of Engineering for Gas Turbines and Power*. 5A: 052506. <https://doi.org/10.1115/1.4035175>.
- Menter F. (1994). Two-equation eddy-viscosity turbulence models for engineering applications. *AIAA Journal*. 32 (8): 1598–1605. <https://doi.org/10.2514/3.12149>.
- Moinier P. (1999). *Algorithm Developments for an Unstructured Viscous Flow Solver*. DPhil Thesis, PhD thesis, University of Oxford.
- Niharika G., Wong T., Ireland P., and Self K. (2016). Study of film cooling in the trailing edge region of a turbine rotor blade in high speed flow using pressure sensitive paint. *Proceedings of ASME Turbo Expo*. 5C: V05CT19A023. <https://doi.org/10.1115/GT2016-57356>.

- O'Dowd D., Zhang Q., He L., Cheong B., and Tibbott I. (2013). Aerothermal performance of a cooled winglet at engine representative mach and reynolds number. *Journal of Turbomachinery*. 135: 011041. <https://doi.org/10.1115/1.4006537>.
- Saul A., Ireland P., Coull J., Wong H., Li H., and Romero E. (2019). An experimental investigation of adiabatic film cooling effectiveness and heat transfer coefficient on a transonic squealer tip. *Journal of Turbomachinery*. 138: 091005. <https://doi.org/10.1115/1.4043263>.
- Vieira J., Coull J., Ireland P., and Romero E. (2021). Aerothermal effect of cavity welding beads on a transonic squealer tip. *Journal of Turbomachinery*. 143: 111009. <https://doi.org/10.1115/1.4051267>.
- Virdi A., Zhang Q., He L., Li H., and Hunsley R. (2015). Aerothermal performance of shroudless turbine blade tips with relative casing movement effects. *Journal of Propulsion and Power*. 31: 527–536. <https://doi.org/10.2514/1.B35331>.
- Wong T., Ireland P., and Self K. (2016). Film cooling effectiveness downstream of trailing edge slots including cutback surface protuberances. *International Journal of Turbomachinery, Propulsion and Power*. 1. <https://doi.org/10.3390/ijtp1010004>.
- Yang Z. and Hu H. (2012). An experimental investigation on the trailing edge cooling of turbine blades. *Journal of Propulsion and Power*. 1: 36–47. <https://doi.org/10.1016/j.jpvr.2012.10.007>.
- Zhang Q., O'Dowd O., He L., Wheeler S., Ligrani M. and Cheong Y. (2011). Overtip shock wave structure and its impact on turbine blade tip heat transfer. *Journal of Turbomachinery*. 133: 041001. <https://doi.org/10.1115/1.4002949>.
- Zhang B., Zhu H., Yao C., and Liu C. (2021). Investigation on aerothermal performance of a rib-slot scheme on the multi-cavity tip of a gas turbine blade. *International Journal of Heat and Mass Transfer*. 176: 121408. <https://doi.org/10.1016/j.ijheatmasstransfer.2021.121408>.
- Zhang B., Yao C., Zhu H., Liu C., and Sunden B. (2022). Experimental study on film cooling performance of a turbine blade tip with a trapezoidal slot cooling scheme in transonic flow using psp technique. *Experimental Thermal and Fluid Science*. 130: 110513. <https://doi.org/10.1016/j.expthermflusci.2021.110513>.